Report

Cell Reports

Prediction of Reach Goals in Depth and Direction from the Parietal Cortex

Graphical Abstract

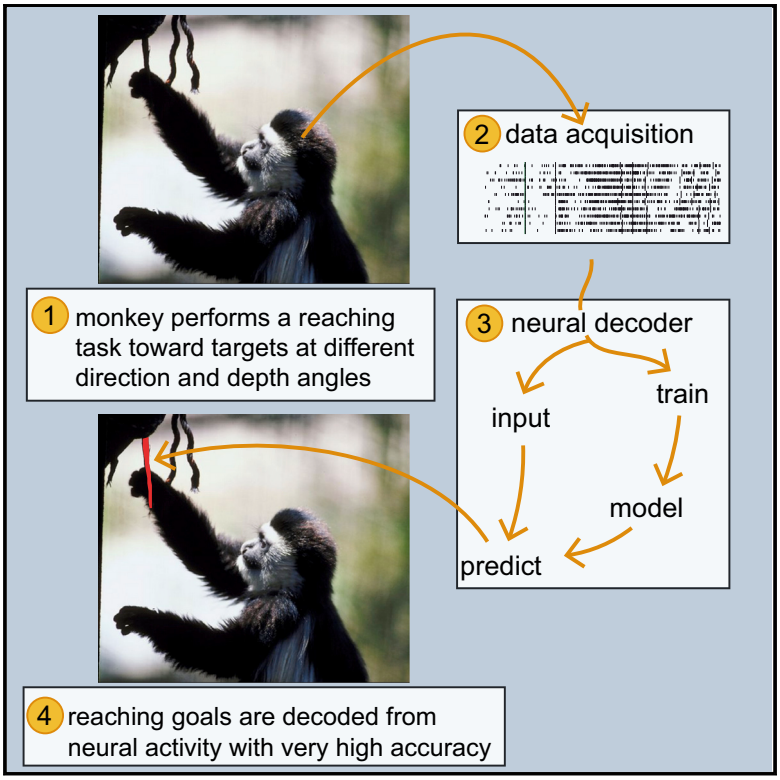

Highlights

- Depths and directions of reaching actions are reliably decoded by the parietal cortex
- Goal locations are discriminated well before movement onset
- The entire prehension action could be decoded from a single cortical site
- Neuroprosthetics from the medial parietal cortex can restore lost reach/grasp functions

Authors

Matteo Filippini, Rossella Breveglieri, Kostas Hadjidimitrakis, Annalisa Bosco, Patrizia Fattori

Correspondence

patrizia.fattori@unibo.it

In Brief

Filippini et al. show that it is possible to use parietal cortex activity to predict in which direction the arm will move and how far it will reach. This opens up the possibility of neural prostheses that can accurately guide reach and grasp using signals from this part of the brain.

Filippini et al., 2018, Cell Reports *23*, 725–732
April 17, 2018
https://doi.org/10.1016/j.celrep.2018.03.090

CellPress

Cell Reports
Report

Prediction of Reach Goals in Depth and Direction from the Parietal Cortex

Matteo Filippini,[1] Rossella Breveglieri,[1] Kostas Hadjidimitrakis,[1,2,3] Annalisa Bosco,[1] and Patrizia Fattori[1,4,*]
[1]University of Bologna Department of Biomedical and Neuromotor Sciences, Bologna, Italy
[2]Biomedicine Discovery Institute and Department of Physiology, Monash University, Clayton, Victoria 3800, Australia
[3]Australian Research Council, Centre of Excellence for Integrative Brain Function, Monash University Node, Clayton, Victoria 3800, Australia
[4]Lead Contact
*Correspondence: patrizia.fattori@unibo.it
https://doi.org/10.1016/j.celrep.2018.03.090

SUMMARY

The posterior parietal cortex is well known to mediate sensorimotor transformations during the generation of movement plans, but its ability to control prosthetic limbs in 3D environments has not yet been fully demonstrated. With this aim, we trained monkeys to perform reaches to targets located at various depths and directions and tested whether the reach goal position can be extracted from parietal signals. The reach goal location was reliably decoded with accuracy close to optimal (>90%), and this occurred also well before movement onset. These results, together with recent work showing a reliable decoding of hand grip in the same area, suggest that this is a suitable site to decode the entire prehension action, to be considered in the development of brain-computer interfaces.

INTRODUCTION

When a spinal cord injury or other diseases do not allow motor commands to reach the muscles, the patient is unable to perform voluntary actions, despite an intact brain. In cases like these, the advent of brain-computer interfaces (BCIs) has offered the possibility to gain control of external devices (neural prostheses) by using the patient's own brain activity (Brandman et al., 2017). Although in the past decade several technical advances provided impressive examples of successful human applications, the performances achieved are still far from enabling widespread clinical application (Cui, 2016). So far, the majority of studies have used primary motor and premotor cortex signals to reconstruct reach trajectories in order to guide robotic limbs in monkeys (Velliste et al., 2008; Wessberg et al., 2000) and humans (Collinger et al., 2013; Hochberg et al., 2012). Although decoding of trajectories is still essential in order to provide the user with natural interfaces, progress in computer vision and robotics is leading to prostheses that do not require trajectory information, as simple algorithms can reconstruct this information from reach endpoint goals (Andersen et al., 2014; Hotson et al., 2016; Katyal et al., 2014).

The posterior parietal cortex (PPC) in humans and monkeys is involved in the sensorimotor transformations required to generate action plans (Andersen et al., 2014; Cui, 2016; Gardner, 2017), so it is a good source for retrieving movement intentions and goals. Pioneering studies demonstrated that reach endpoints (Musallam et al., 2004; Serruya et al., 2003), trajectories (Mulliken et al., 2008; Figure 1A), and grips (Schaffelhofer et al., 2015; Figure 1A) can be extracted from monkey PPC. Translational work in humans produced similar results (Aflalo et al., 2015; Figure 1B), together with reliable hand shape decoding (Klaes et al., 2015; Figure 1B). In the aforementioned studies, reaches were performed on a single plane. To the best of our knowledge, only one study in monkey PPC performed decoding of reach goal and trajectory information in a virtual three-dimensional (3D) environment (Hauschild et al., 2012).

A medial PPC area termed V6A (Figure 1A) is known to encode not only goals and reach movement directions (Bosco et al., 2010, 2016; Breveglieri et al., 2014; Hadjidimitrakis et al., 2014) but also several grasping parameters (Fattori et al., 2017). Previous research suggested that V6A could integrate the arm transport and hand grip components of a reach-to-grasp action. (Galletti and Fattori, 2018). Although a reliable decoding of hand grip from V6A signals has recently been shown (Filippini et al., 2017), decoding of reach-related information has not yet been performed (Figure 1A). We addressed this issue, with the aim of finding a parietal region where both grasping and reaching signals can be decoded. In a different way to most previous related studies, we varied reaches not only on a frontoparallel plane but using a naturalistic environment also involving depth (distance from the body).

RESULTS

Data were recorded from two monkeys while they performed a fixation-to-reach task toward nine spatial positions with three different direction angles and three different depth levels (Figure 1C), covering a wide range of positions in peripersonal space. Target elevation was kept constant, at eye level. We sequentially recorded 264 V6A cells, 181 neurons in monkey 1 (M1) and 83 in monkey 2 (M2). Parts of this dataset have already been published in previous studies aimed at exploring the encoding of depth and direction in V6A activity (Hadjidimitrakis et al., 2014, 2017). The population discharge of the whole dataset is shown in Figure S1A. The plot shows a clear distinction among the activations during the early vision of the target, then during the preparation, and finally during the execution of reaching action. Moreover, Figure S1A shows

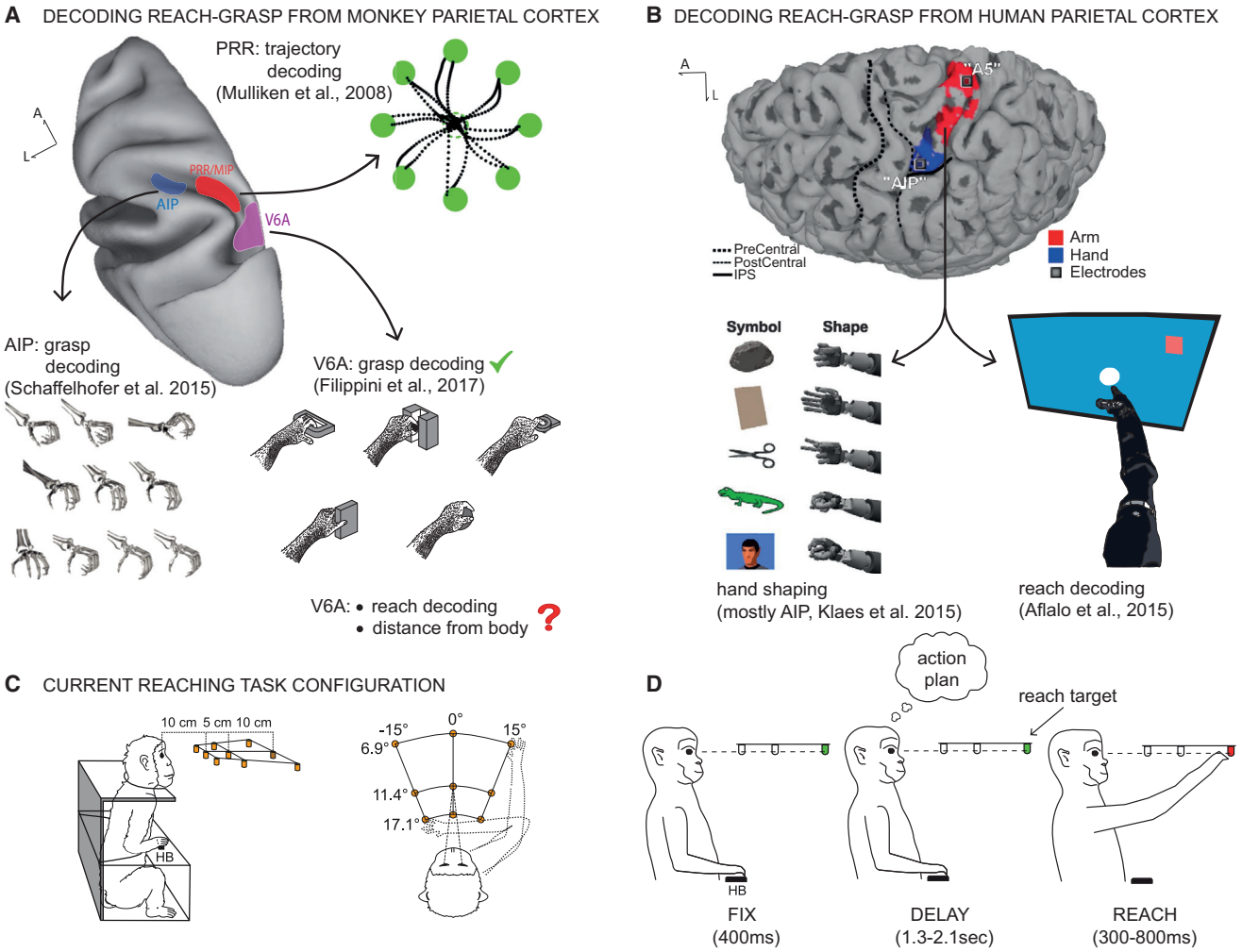

Figure 1. Decoding Reach-Grasp Action from Parietal Cortex and Task Paradigm

(A) Decoding for reaching and grasping by the monkey posterior parietal cortex. Top left: dorsal view of the left hemisphere of a macaque brain. Highlighted hotspots in the parietal cortex represent areas used in recent literature to extract signals useful to decode grasp (anterior intraparietal [AIP] area from Schaffelhofer et al., 2015) and/or movement trajectories (parietal reach region [PRR] and medial intraparietal area [MIP]; from Mulliken et al., 2008). V6A signals have recently been used to decode grasping (Filippini et al., 2017). The goal of the present study was to decode reaching targets by the V6A. A, anterior; L, lateral.

(B) Decoding in the human posterior parietal cortex for reach on a frontal plane (Aflalo et al., 2015) and hand shapes (Klaes et al., 2015) separately. Modified from Aflalo et al. (2015) and Klaes et al. (2015). A5, Brodmann's area 5.

(C) Scheme of the setup used for the task in the present study. Left: nine LEDs that were used as fixation and reaching targets (orange) were located at eye level. The distances from the eyes of the three targets of the central row are shown. HB, home button. Right: top view of the target configuration showing the values of version (top) and vergence angles (left). Targets in different positions on the horizontal axis have a different laterality (direction); on the vertical axis, targets change in distance from the body (depth).

(D) Cartoon of the fixation-to-reach task performed by monkeys. Left: in the first part of the task (fix epoch), the monkey had to fixate one of nine targets. In the delay epoch (center) the monkey had to maintain fixation on the target and wait for the go signal (i.e., target color changing from green to red) while planning the action. Right: in the reach epoch, the monkey released the home button to perform the reaching movement toward the target.

that the V6A neural population starts discriminating among different targets as soon as the LED is illuminated. The discrimination power of the population increases slightly when the monkey is preparing the action (epoch delay, from 450 ms after the fixation onset to the arm movement onset), and has a second peak when the action is executed (reach). Population tuning properties were confirmed using a sliding-window ANOVA (Figure S1B).

Whole-Epoch Decoding

The activity of each neuron was quantified in the three main epochs depicted in Figure 1D: fix, delay, and reach, corresponding to the period of early fixation of the target, the planning phase of the subsequent reach action, and the execution phase, respectively. Subsequently, population decoding analysis was performed using a naive Bayes classifier (see Experimental Procedures). The results are presented separately for

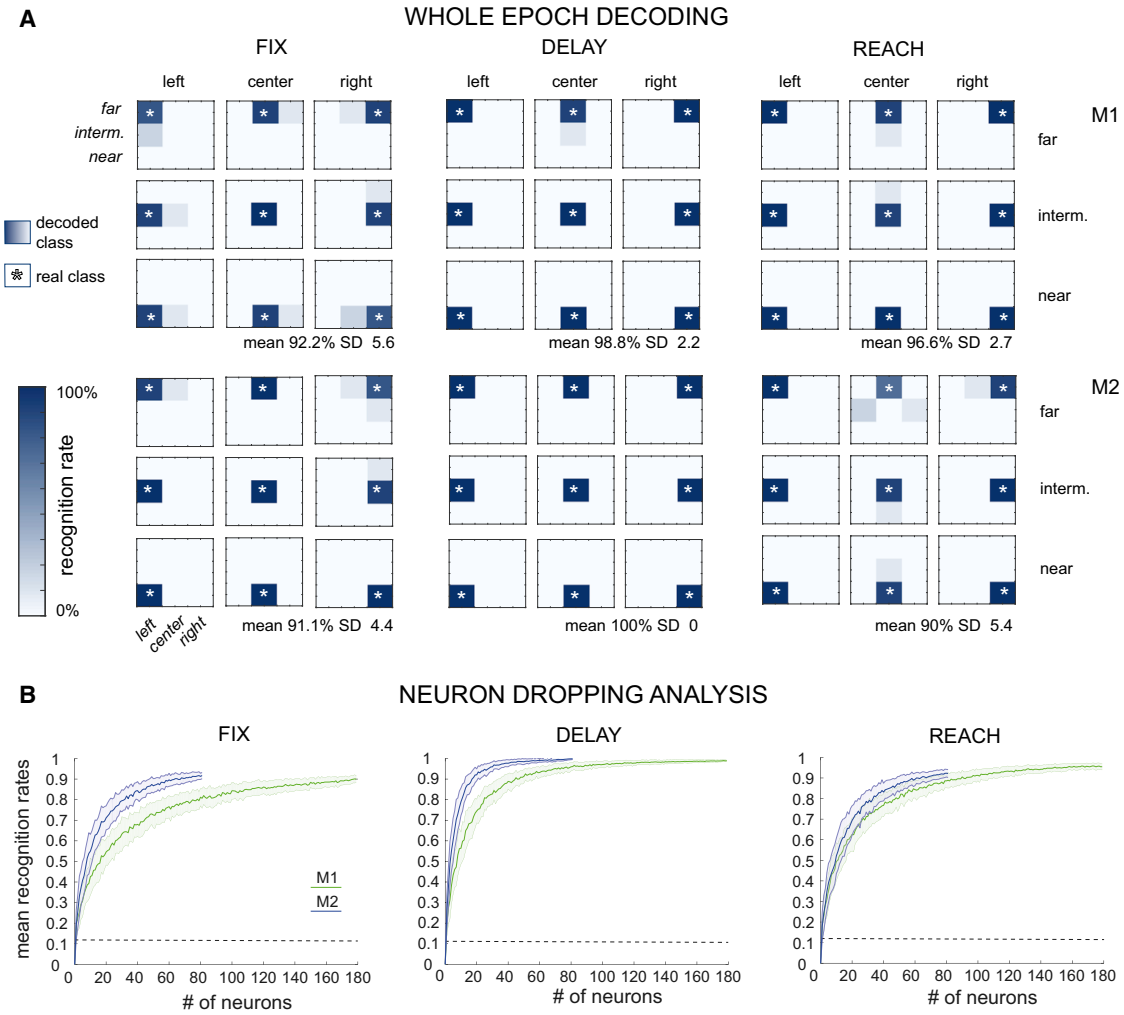

Figure 2. Decoding Accuracy of Reach Goals Location from V6A Signals

(A) Whole-epoch decoding. Confusion matrices describing the pattern of errors made by the naive Bayes classifier in the recognition of target positions. Mean firing rates were calculated for different epochs (left, fix; center, delay; right, reach) and monkeys (first row, monkey 1 [M1]; middle row, monkey 2 [M2]). In each 3 × 3 sub-matrix, the actual goal location is indicated as a white asterisk according to its position in the monkey's workspace (near/intermediate/far and left/central/right). For each real class, decoder predictions (recognition rate) were plotted with a color scale. Mean recognition rates are reported together with SDs below the indices. These matrices show the highly successful decoding and that the few not perfect classifications involve spatially close target positions.

(B) Neuron-dropping analysis. Accuracy of decoding as a function of the number of neurons included in the analysis. Dotted line, chance level (0.11). For each step (zero to neurons available per monkey), we randomly caught an increasing number of neurons from the pool, to include in the analysis. This procedure was repeated 100 times per step to calculate SD values. Results are shown for the two cases (green, M1; blue, M2) and the three epochs analyzed. All in all, it is evident that a maximum of 20–40 neurons is required to efficiently decode reach goals.

the two monkeys. In each monkey, all recorded cells were included in the analysis, irrespectively of whether they responded differently depending on the position of the target or not.

Our decoder correctly classified target positions well before movement onset: we found a high correlation between the actual and the decoded spatial positions during fix (Figure 2A). The mean accuracies, obtained using a ''leave-p-out'' 5-fold cross-validation (p value 20% of trials), were excellent in both monkeys (91%–92%) and well above chance level (11%, the conditions being nine). Misclassifications were very few and occurred between adjacent targets. The decoding accuracies during both reach planning (delay) and execution (reach) were even higher than during fix, again in both monkeys.

Neuron-Dropping Analysis

Figure 2B depicts the decoding accuracy as a function of the population size. Results varied across epochs and monkeys: in fix (Figure 2B, left), a sample of 20–40 neurons (median 40) was sufficient to achieve 70% accuracy, whereas in reach (Figure 2B, right), 20–30 neurons (median 26) were required, and in delay (Figure 2B, center), between 10 and 20 neurons (median 15) were required. In all cases, a small number of neurons was enough to obtain accurate decoding.

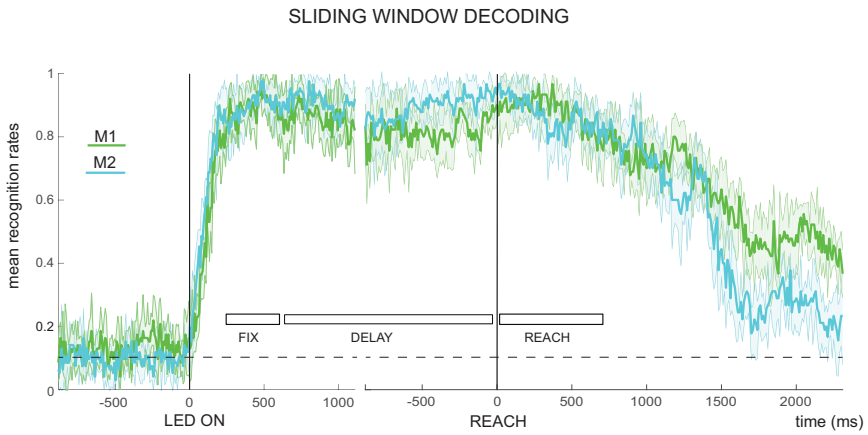

Figure 3. Sliding-Window Decoding Analysis

Time course of the decoding accuracy (recognition rates) on the basis of the firing rates extracted during the period starting 1 s before the target illumination (LED on), until 2 s after the movement onset (reach). Because of the variable duration of the delay interval (1.3–2.1 s), double-alignment result plots are shown. Firing rates were calculated for a 300 ms sliding window, moving forward with a 10 ms step. Each dot on the graph was plotted at the beginning of the 300 ms window. The mean lines were calculated as the arithmetic mean between recognition rates of individual target positions. For each position, variability bands are shown, representing SDs on the basis of a 5-fold cross-validation.

Time Course of the Decoding Performance

To evaluate the temporal evolution of decoding accuracy, we estimated the decoding performance using activity in smaller time intervals compared with the whole epochs. A rapid increase of the decoding performance, occurring around the time of the LED onset (LED on), is evident in Figure 3. At fixation onset (fix epoch), the recognition rate reached its peak and remained constant in the subsequent delay interval (delay) and in the reaching execution (reach). Interestingly, after the reaching, the gaze and the hand still remained on the target, whereas the decoding accuracy decreased. This suggests that the decoding performance is strictly linked to the preparation and execution of reaching, instead of being linked to the gaze fixation of the target, as documented by decoding results shown from a control experiment in Figure S2. In the task used in the main text (Figures 1C and 1D), gaze position and reach goal were coincident. Rather than related to reach goals, one could argue that the predictions of our classifier were related to gaze position-related and/or reach preparation-related activity (Breveglieri et al., 2012, 2014; Hadjidimitrakis et al., 2011, 2012). To uncouple the decoding of gaze and reach goals, 67 neurons out of 83 of the original population were recorded while M2 performed a delayed reaching task toward the same nine targets of the original task with the gaze fixed on the central position (constant-gaze task). A yellow flash (cue), in the early phase of the delay, instructed the monkey as to which target should be reached for. In the constant-gaze task, the increase of tuned cells occurs at cue onset (i.e., when the monkey receives instruction about the location of the target to be subsequently reached for). On the contrary, in the same neurons (n = 67) tested in the fixation-to-reach task, the increase of tuned cells occurred at the fixation onset, because in this task the fixation LED per se instructed the monkey about the reach goal location. The same trend was also observed in the decoding performance: the accuracy was very low during fixation before the cue and increased immediately after the cue was given. This rules out the possibility that gaze fixation per se is responsible for the high decoding performance achieved in the fixation-to-reach task. The accuracy shown in the confusion matrices from the constant-gaze task is not significantly different from the results of the same population of cells when tested for the fixation-to-reach task (results for the fixation-to-reach task for the 67 cells tested for both tasks: 90% [SD 4.1%] for fix epoch, 98% [SD 2.2%] for delay epoch, and 88% [SD 4.9%] for reach epoch, t-test $p > 0.05$). Neuron-dropping and sliding-window analyses (Figures S2D and S2E) support the evidence that as soon as the visual cue was provided, the decoding performance reached optimal values for both constant-gaze and fixation-to-reach tasks. The data of the control experiment highlight that gaze information is not necessary to obtain high decoding accuracy from area V6A.

Generalization Analysis

To evaluate whether the neural code used during the early fixation period was retained or changed during the subsequent planning interval before the reach movement, we performed a generalization analysis by training decoders in either the fix or the reach epoch, then we applied both codes on these epochs and portions of the delay epoch. Figure 4 shows the results of this analysis for the two monkeys. The code learned during the early fixation period (fix, blue line) was gradually lost in the delay intervals; the accuracy then dropped during movement execution (~20%). This suggests that the neural code used during the earliest fixation phase became progressively weaker as soon as the animal began to prepare the movement. The time course of the accuracy obtained by training the algorithm with the movement neural activity (reach, red line in Figure 4), and testing the algorithm with the delay activity demonstrated that the neural code used during the action execution was partially preserved also during the last part of the planning period, but not in the earlier planning phases and initial fixation. In summary, by looking at the activity during early fixation, it was not possible to predict the spatial position during reach execution, and vice versa. When the accuracy of the classifier trained in the different fractions of the delay was analyzed (Figures 4C and 4D, gray lines), progressive code transformations were present. Both monkeys depicted a smooth transition between an earlier code, possibly related to the gaze location information, and a later code correlated with the movement preparation.

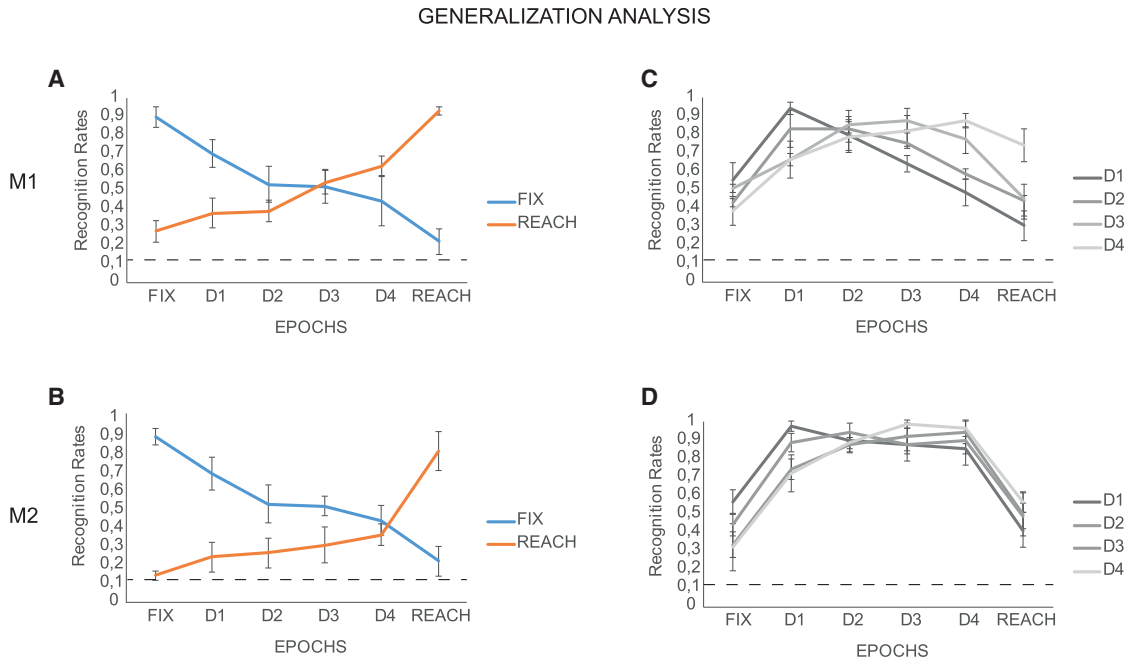

Figure 4. Generalization Analysis

(A–D) Generalization of codes derived from different epochs: the decoder was trained with the mean firing rates during one epoch and then tested to decode the other epochs. The trend of mean recognition rates together with the SD bars through different epochs are plotted as colored lines. Results are shown for the two monkeys M1 (A and C) and M2 (B and D). The delay epoch was split in portions because of variable time duration between the trials: D1, 0%–25% of the delay epoch; D2, 25%–50%; D3, 50%–75%; and D4, 75%–100%. Blue line shows the decoder trained on fix, and red line shows the decoder trained on reach (A and B). The decoder was trained on fractions (different gray scales) of the delay epoch (C and D).

DISCUSSION

In this study, we demonstrated that neural signals from area V6A can be successfully used for the offline decoding of reach goals located at different depths and directions, in conditions similar to everyday life, in which reaching movements are performed not only on a single plane but also in three dimensions. In most cases, just a few neurons (~20) were sufficient to achieve a correct prediction. The accuracy of decoding was optimal from early target fixation to the end of reaching.

We used a task configuration in which the monkeys fixated the goal of reaching movement, which is the most physiological condition (Hayhoe et al., 2003; Neggers and Bekkering, 2001). However, this setup cannot distinguish whether decoding uses gaze signals or arm movement-related activity. To exclude gaze-related activity from decoded signals, we performed decoding in another experiment in which the monkey performed a task in which gaze and reaching targets were not coincident (Figure S2). In this case too, decoding performance was very high. This result is in line with the strong spatial tuning in V6A reach-related activity when gaze is dissociated from the reach target position (Bosco et al., 2016). However, in our study, we did not test decoding in a free-gaze condition, in which gaze was truly independent. Thus, we cannot exclude the possibility that eye movements could potentially disturb the decoding from V6A. However, the very similar results obtained between tasks (Figures 3 and S2E) suggest that free gaze should not interfere with decoding reliability from V6A. Nevertheless, these results suggest V6A as a source for BCIs, not only when the patient can move his or her eyes to the reaching target but also in the absence of ocular motility.

Decoding Reach Goals from Parietal Cortex

Several monkey studies performed decoding of reach goals (Musallam et al., 2004; Scherberger et al., 2005; Shenoy et al., 2003) and trajectories (Mulliken et al., 2008) in two-dimensional (2D) space from activity in PPC (specifically, from the parietal reach region [PRR]). Here, we decoded reach goal from another part of PPC, while also considering the depth dimension.

In V6A, target location was decoded from neural responses occurring not only during reaching execution but also well before movement onset. This is similar to the neighboring PRR area, where neural signals during reach planning were used to online decode up to six reach goals on a screen and to guide a cursor (Musallam et al., 2004). Accuracy obtained in PRR was lower than in V6A (from 25% to 60% in PRR [Musallam et al., 2004] versus about 90%–100% in V6A [present results]). However, differences in the experimental design may account for these discrepancies.

Here, the trajectory of the reaching movement could not be extracted, because only information on the reach goal location was available. Nevertheless, it was demonstrated that goal specificity is advantageous for ballistic operations (Musallam et al., 2004) and that by incorporating information about the reach

goal (target position), the decoding accuracy of the trajectory estimation from PRR signals improved by 17% (goal-based Kalman filter; Mulliken et al., 2008). Alternatively, the optimal reconstruction of movement trajectories could be performed by computer vision (Andersen et al., 2014; Katyal et al., 2014).

Looking at current state-of-the-art neural prosthesis technology, in order to increase prosthesis reliability, we need to increment the number of neurons sampled. This involves overcoming several technical limitations and using more invasive implants. Intuitively, a mixed neural signals-computer vision-driven BCI looks more feasible. From the PPC region, we can retrieve intention of movements, and this information could aid computer vision systems to be "mind controlled" or classic motor BCIs (i.e., BCIs driven by motor cortex) to reconstruct the movement smoothly, knowing movement goals in advance. Exploiting higher order, multidimensional information for decoding purposes could allow the development of more natural and user-friendly brain-machine interfaces to achieve fully integrated prehensile actions.

Decoding of Depth Information for Reaching

This study shows the decoding of reaching goals from signals in PPC, also taking into account the depth dimension. Several studies demonstrated the feasibility of retrieving instantaneous movement attributes, such as position, velocity, and acceleration useful to drive artificial limbs in 3D space (Brandman et al., 2017). This has been achieved using activity from motor and premotor regions in monkeys (Carmena et al., 2003; Jarosiewicz et al., 2008; Taylor et al., 2002; Velliste et al., 2008) and in humans (Collinger et al., 2013; Hochberg et al., 2012). In monkey PPC (areas PRR and 5d), continuous trajectory reconstruction of cursor movements in a 3D virtual space was demonstrated by Hauschild et al. (2012). In that study, a good decoding performance ($R^2 \sim 40\%$) was obtained using ensembles of about sixty neurons.

BCI applications that restore basic interaction with objects in tetraplegic patients have recently been reported (Aflalo et al., 2015; Collinger et al., 2013; Hochberg et al., 2012). These studies demonstrated the feasibility of BCIs in humans, but there is much work still to be done. When the depth information was added, movements became reasonably slower and clumsier (Collinger et al., 2013). Thus, our results showing reliable decoding not only in two dimensions but also in depth are of particular importance.

Decoding Entire Prehension from V6A

V6A has recently been suggested as a site of convergence of arm signals for reaching and grip signals for grasping to direct our hands toward efficient prehensile actions (Galletti and Fattori, 2018; Gardner, 2017). In humans, fMRI signals from a region that is a likely homolog of monkey V6A (Pitzalis et al., 2013) were used to successfully predict the direction of an upcoming reach, but not of a saccade (Gallivan et al., 2011). In a recent study, Nelissen et al. (2018) decoded grasping-related information from fMRI signals in monkey area V6A. This finding complements the decoding of the type of grasp (Filippini et al., 2017) and reach goals (present results) and suggests that V6A could be a useful site for the neuroprosthetic control of the entire prehension action.

Potential Applications and Future Directions

Despite the tremendous advances in neural prosthetics on the basis of signals from the motor cortex, the future of BCIs relies on the acquisition of neural signals that also reflect the cognitive state of the patient (i.e., intentions and movement goals) (Andersen et al., 2014). These cognitive prostheses may be implemented by decoding neural signals from parietal regions, such as V6A, so as to have signals related to movement intention and execution from the same area. V6A incorporates signals typical of parietal regions (intentions of movement) but also signals coding for some useful details of the movement, such as depth and direction of reaching, and even grip type (Filippini et al., 2017). These intelligent prosthetics are one potential application of the results presented here.

Another potential and promising application of decoding arm actions from V6A is in the emerging field of soft robotics, a technology born mimicking natural beings, to replace classical rigid-bodied robots with limbs that are more comfortable and easy to handle (Rus and Tolley, 2015). Although soft robotics is becoming more and more popular, the potential of soft machines in the clinical field is still greatly under-exploited, mainly because of limited functionality and versatility caused by the lack of intelligent, natural control systems. Indeed, so far soft robots have relied on classic control approaches that reduce the advantages of "soft" robotics in terms of flexible interaction with a variable environment. A direction for the very near future is to design more intelligent soft robots taking advantage of bio-inspired controllers that will be developed thanks to advances in artificial intelligence and inspired by the neurophysiology of our bodies (Fani et al., 2016; Santello et al., 2016). For a new generation of user-friendly prostheses such as these biomorphic robots, natural signals with multiple neural information such as those from V6A might be exploited for a more dexterous control of artificial limbs.

EXPERIMENTAL PROCEDURES

The study was performed in accordance with the guidelines of European Union (EU) directives (86/609/EEC and 2010/63/EU) and Italian national laws (D.L. 116-92 and D.L. 26-2014) on the protection of animals used for scientific purposes. Protocols were approved by the Animal-Welfare Body of the University of Bologna. During training and recording sessions, particular attention was paid to any behavioral and clinical sign of pain or distress. For surgical and electrophysiological procedures, see Hadjidimitrakis et al. (2014). Two male monkeys (M1 and M2, aged 5 and 8 years) were involved in the study.

Equipment and Behavioral Task

Electrophysiological data were collected while monkeys were performing a fixation-to-reach task with the contralateral limb (with respect to the recording hemisphere), with the head restrained, in darkness, while maintaining steady fixation of the target. Reaches were performed to one of nine light-emitting diodes (LEDs; 6 mm in diameter; Figure 1C). The LEDs were mounted on a panel located in front of the animal, at different distances and directions with respect to the eyes, but always at eye level.

Given that the interocular distance for both animals was 30 mm, the nearest targets were located at 10 cm from the eyes, whereas the LEDs placed at intermediate and far positions were at a distance of 15 and 25 cm, respectively. Because targets were aligned at eye level, they could potentially obscure each other. We solved the problem by masking the nearest LEDs to be visibly thinner than second-line LEDs and the latter thinner than the farthest line. Thus, the monkeys were able to easily discriminate them.

In the task, the monkeys pressed a button located close to their chest (home button [HB]; Figure 1C), fixated one of the targets for a variable period (fix; Figure 1D, left), prepared the movement (delay; Figure 1D, center), and started the reaching movement (reach, Figure 1D, right) toward the foveated target.

Data Analysis

The analyses were performed with customized scripts in MATLAB (The MathWorks; RRID: SCR_001622) and Python (using open-source machine learning toolkit scikit-learn, http://scikit-learn.org; RRID: SCR_002577). The neural activity was analyzed by quantifying the discharge in each trial in the following three different epochs (Figure 1D): (1) the early fixation epoch (fix), from 50 ms after the end of the saccade performed to gaze at the LED until 450 ms after it; (2) the preparation epoch (delay), from 450 ms after the end of the saccade to the arm movement onset (given the task structure and the variable reaction time of the monkeys, this epoch had a variable duration from about 1.3 to 2.1 s); and (3) the reach epoch (reach), from arm movement onset (M) until the end of it, signaled by the pressing of the LED target.

All analyses and modeling were done offline. Among the original set of recorded neurons, we considered only cells with at least ten trials for each of the nine targets. All recorded neurons, either modulated in the reaching task or not (see Supplemental Experimental Procedures), were used in the decoding analysis.

Neural Decoding

For each neuron of the population (181 neurons for M1, 83 for M2, respectively), we computed the mean firing rate (mFR; number of spikes per time unit) over a selected time span using a trial-by-trial approach. The decoder outputs were the nine targets. Fivefold cross-validation was performed by using 72 samples (8 for each condition) for training and 18 (2 for each condition) for testing for each neuron, to ensure that the classifier was trained and tested on different data. Recognition rates and SDs were calculated as means over the five folds' iterations. Not normalized data were used for the decoding procedure.

We used a naive Bayesian classifier as decoding algorithm. Naive Bayes methods are a set of supervised learning algorithms based on applying Bayes' theorem with the "naive" assumption of independence between every pair of features. This technique has been shown to achieve performance closer to optimal compared with other classifiers such as support vector machine (SVM) when analyzing neural data (Carpaneto et al., 2011; Schaffelhofer et al., 2015). In our Python custom scripts, we implemented the module of naive Bayes classifiers proposed by scikit-learn libraries (the statistical formulation can be found at http://scikit-learn.org/stable/modules/naive_bayes.html; Zhang, 2004). Under the assumption of Poisson distribution of features, we reinforced the model as suggested at the following site: http://github.com/scikit-learn/scikit-learn/pull/3708/files (Ma et al., 2006). We performed three types of analysis, computing the following feature vectors over different epochs and time spans: whole-epoch, sliding-window, and generalization analysis. The same kinds of analyses have been performed in area V6A from different sets of neurons recorded in a grasping task (Filippini et al., 2017).

DATA AND SOFTWARE AVAILABILITY

The MATLAB and Python scripts reported in this paper are available at Mendeley Data: https://doi.org/10.17632/jsf27x5pk4.1.

SUPPLEMENTAL INFORMATION

Supplemental Information includes Supplemental Experimental Procedures and two figures and can be found with this article online at https://doi.org/10.1016/j.celrep.2018.03.090.

ACKNOWLEDGMENTS

We wish to thank Massimo Verdosci and Francesco Campisi for technical assistance and Michela Gamberini and Lauretta Passarelli for surgical procedures and anatomical reconstructions. This study was supported by Ministero dell'Università e della Ricerca (Italy), FIRB 2013 N. RBFR132BKP (Italy), National Health and Medical Research Council grant APP1082144 (Australia), and European Union H2020-MSCA-734227 – PLATYPUS.

AUTHOR CONTRIBUTIONS

Conceptualization, P.F.; Data Curation Management Activities, M.F. and R.B.; Formal Analysis Application, M.F.; Funding Acquisition, P.F. and A.B.; Investigation Conduct, R.B., A.B., and K.H.; Methodology Development or Design of Methodology, M.F.; Project Administration Management, P.F.; Resources Provision of Study Materials, P.F. and A.B.; Software Programming, Software Development, M.F.; Supervision Oversight, P.F.; Validation Verification, P.F., K.H., and R.B.; Visualization Preparation, M.F. and R.B.; Writing – Original Draft, M.F. and R.B.; Writing – Review & Editing, M.F., K.H., R.B., and P.F.

DECLARATION OF INTERESTS

The authors declare no competing interests.

Received: September 8, 2017
Revised: February 3, 2018
Accepted: March 20, 2018
Published: April 17, 2018

REFERENCES

Aflalo, T., Kellis, S., Klaes, C., Lee, B., Shi, Y., Pejsa, K., Shanfield, K., Hayes-Jackson, S., Aisen, M., Heck, C., et al. (2015). Neurophysiology. Decoding motor imagery from the posterior parietal cortex of a tetraplegic human. Science *348*, 906–910.

Andersen, R.A., Kellis, S., Klaes, C., and Aflalo, T. (2014). Toward more versatile and intuitive cortical brain-machine interfaces. Curr. Biol. *24*, R885–R897.

Bosco, A., Breveglieri, R., Chinellato, E., Galletti, C., and Fattori, P. (2010). Reaching activity in the medial posterior parietal cortex of monkeys is modulated by visual feedback. J. Neurosci. *30*, 14773–14785.

Bosco, A., Breveglieri, R., Hadjidimitrakis, K., Galletti, C., and Fattori, P. (2016). Reference frames for reaching when decoupling eye and target position in depth and direction. Sci. Rep. *6*, 21646.

Brandman, D.M., Cash, S.S., and Hochberg, L.R. (2017). Review: human intracortical recording and neural decoding for brain-computer interfaces. IEEE Trans. Neural Syst. Rehabil. Eng. *25*, 1687–1696.

Breveglieri, R., Hadjidimitrakis, K., Bosco, A., Sabatini, S.P., Galletti, C., and Fattori, P. (2012). Eye position encoding in three-dimensional space: integration of version and vergence signals in the medial posterior parietal cortex. J. Neurosci. *32*, 159–169.

Breveglieri, R., Galletti, C., Dal Bò, G., Hadjidimitrakis, K., and Fattori, P. (2014). Multiple aspects of neural activity during reaching preparation in the medial posterior parietal area V6A. J. Cogn. Neurosci. *26*, 878–895.

Carmena, J.M., Lebedev, M.A., Crist, R.E., O'Doherty, J.E., Santucci, D.M., Dimitrov, D.F., Patil, P.G., Henriquez, C.S., and Nicolelis, M.A.L. (2003). Learning to control a brain-machine interface for reaching and grasping by primates. PLoS Biol. *1*, E42.

Carpaneto, J., Umiltà, M.A., Fogassi, L., Murata, A., Gallese, V., Micera, S., and Raos, V. (2011). Decoding the activity of grasping neurons recorded from the ventral premotor area F5 of the macaque monkey. Neuroscience *188*, 80–94.

Collinger, J.L., Wodlinger, B., Downey, J.E., Wang, W., Tyler-Kabara, E.C., Weber, D.J., McMorland, A.J.C., Velliste, M., Boninger, M.L., and Schwartz, A.B. (2013). High-performance neuroprosthetic control by an individual with tetraplegia. Lancet *381*, 557–564.

Cui, H. (2016). Forward prediction in the posterior parietal cortex and dynamic brain-machine interface. Front. Integr. Nuerosci. *10*, 35.

Fani, S., Bianchi, M., Jain, S., Pimenta Neto, J.S., Boege, S., Grioli, G., Bicchi, A., and Santello, M. (2016). Assessment of myoelectric controller performance

and kinematic behavior of a novel soft synergy-inspired robotic hand for prosthetic applications. Front. Neurorobot. *10*, 11.

Fattori, P., Breveglieri, R., Bosco, A., Gamberini, M., and Galletti, C. (2017). Vision for prehension in the medial parietal cortex. Cereb. Cortex *27*, 1149–1163.

Filippini, M., Breveglieri, R., Akhras, M.A., Bosco, A., Chinellato, E., and Fattori, P. (2017). Decoding information for grasping from the macaque dorsomedial visual stream. J. Neurosci. *37*, 4311–4322.

Galletti, C., and Fattori, P. (2018). The dorsal visual stream revisited: stable circuits or dynamic pathways? Cortex *98*, 203–217.

Gallivan, J.P., McLean, D.A., Valyear, K.F., Pettypiece, C.E., and Culham, J.C. (2011). Decoding action intentions from preparatory brain activity in human parieto-frontal networks. J. Neurosci. *31*, 9599–9610.

Gardner, E.P. (2017). Neural pathways for cognitive command and control of hand movements. Proc. Natl. Acad. Sci. U S A *114*, 4048–4050.

Hadjidimitrakis, K., Breveglieri, R., Placenti, G., Bosco, A., Sabatini, S.P., and Fattori, P. (2011). Fix your eyes in the space you could reach: neurons in the macaque medial parietal cortex prefer gaze positions in peripersonal space. PLoS ONE *6*, e23335.

Hadjidimitrakis, K., Breveglieri, R., Bosco, A., and Fattori, P. (2012). Three-dimensional eye position signals shape both peripersonal space and arm movement activity in the medial posterior parietal cortex. Front. Integr. Neurosci. *6*, 37.

Hadjidimitrakis, K., Bertozzi, F., Breveglieri, R., Bosco, A., Galletti, C., and Fattori, P. (2014). Common neural substrate for processing depth and direction signals for reaching in the monkey medial posterior parietal cortex. Cereb. Cortex *24*, 1645–1657.

Hadjidimitrakis, K., Bertozzi, F., Breveglieri, R., Galletti, C., and Fattori, P. (2017). Temporal stability of reference frames in monkey area V6A during a reaching task in 3D space. Brain Struct. Funct. *222*, 1959–1970.

Hauschild, M., Mulliken, G.H., Fineman, I., Loeb, G.E., and Andersen, R.A. (2012). Cognitive signals for brain-machine interfaces in posterior parietal cortex include continuous 3D trajectory commands. Proc. Natl. Acad. Sci. U S A *109*, 17075–17080.

Hayhoe, M.M., Shrivastava, A., Mruczek, R., and Pelz, J.B. (2003). Visual memory and motor planning in a natural task. J. Vis. *3*, 49–63.

Hochberg, L.R., Bacher, D., Jarosiewicz, B., Masse, N.Y., Simeral, J.D., Vogel, J., Haddadin, S., Liu, J., Cash, S.S., van der Smagt, P., and Donoghue, J.P. (2012). Reach and grasp by people with tetraplegia using a neurally controlled robotic arm. Nature *485*, 372–375.

Hotson, G., Smith, R.J., Rouse, A.G., Schieber, M.H., Thakor, N.V., and Wester, B.A. (2016). High precision neural decoding of complex movement trajectories using recursive Bayesian estimation with dynamic movement primitives. IEEE Robot. Autom. Lett. *1*, 676–683.

Jarosiewicz, B., Chase, S.M., Fraser, G.W., Velliste, M., Kass, R.E., and Schwartz, A.B. (2008). Functional network reorganization during learning in a brain-computer interface paradigm. Proc. Natl. Acad. Sci. U S A *105*, 19486–19491.

Katyal, K.D., Johannes, M.S., Kellis, S., Aflalo, T., Klaes, C., McGee, T.G., Para, M.P., Shi, Y., Lee, B., Pejsa, K., et al. (2014). A collaborative BCI approach to autonomous control of a prosthetic limb system. In Proceedings of the IEEE International Conference on Systems, Man and Cybernetics, pp. 1479–1482.

Klaes, C., Kellis, S., Aflalo, T., Lee, B., Pejsa, K., Shanfield, K., Hayes-Jackson, S., Aisen, M., Heck, C., Liu, C., and Andersen, R.A. (2015). Hand shape representations in the human posterior parietal cortex. J. Neurosci. *35*, 15466–15476.

Ma, W.J., Beck, J.M., Latham, P.E., and Pouget, A. (2006). Bayesian inference with probabilistic population codes. Nat. Neurosci. *9*, 1432–1438.

Mulliken, G.H., Musallam, S., and Andersen, R.A. (2008). Decoding trajectories from posterior parietal cortex ensembles. J. Neurosci. *28*, 12913–12926.

Musallam, S., Corneil, B.D., Greger, B., Scherberger, H., and Andersen, R.A. (2004). Cognitive control signals for neural prosthetics. Science *305*, 258–262.

Neggers, S.F., and Bekkering, H. (2001). Gaze anchoring to a pointing target is present during the entire pointing movement and is driven by a non-visual signal. J. Neurophysiol. *86*, 961–970.

Nelissen, K., Fiave, P.A., and Vanduffel, W. (2018). Decoding grasping movements from the parieto-frontal reaching circuit in the nonhuman primate. Cereb. Cortex *28*, 1245–1259.

Pitzalis, S., Sereno, M.I., Committeri, G., Fattori, P., Galati, G., Tosoni, A., and Galletti, C. (2013). The human homologue of macaque area V6A. Neuroimage *82*, 517–530.

Rus, D., and Tolley, M.T. (2015). Design, fabrication and control of soft robots. Nature *521*, 467–475.

Santello, M., Bianchi, M., Gabiccini, M., Ricciardi, E., Salvietti, G., Prattichizzo, D., Ernst, M., Moscatelli, A., Jorntell, H., Kappers, A.M.L., et al. (2016). Towards a synergy framework across neuroscience and robotics: lessons learned and open questions. Reply to comments on: "Hand synergies: Integration of robotics and neuroscience for understanding the control of biological and artificial hands". Phys. Life Rev. *17*, 54–60.

Schaffelhofer, S., Agudelo-Toro, A., and Scherberger, H. (2015). Decoding a wide range of hand configurations from macaque motor, premotor, and parietal cortices. J. Neurosci. *35*, 1068–1081.

Scherberger, H., Jarvis, M.R., and Andersen, R.A. (2005). Cortical local field potential encodes movement intentions in the posterior parietal cortex. Neuron *46*, 347–354.

Serruya, M., Hatsopoulos, N., Fellows, M., Paninski, L., and Donoghue, J. (2003). Robustness of neuroprosthetic decoding algorithms. Biol. Cybern. *88*, 219–228.

Shenoy, K.V., Meeker, D., Cao, S., Kureshi, S.A., Pesaran, B., Buneo, C.A., Batista, A.P., Mitra, P.P., Burdick, J.W., and Andersen, R.A. (2003). Neural prosthetic control signals from plan activity. Neuroreport *14*, 591–596.

Taylor, D.M., Tillery, S.I.H., and Schwartz, A.B. (2002). Direct cortical control of 3D neuroprosthetic devices. Science *296*, 1829–1832.

Velliste, M., Perel, S., Spalding, M.C., Whitford, A.S., and Schwartz, A.B. (2008). Cortical control of a prosthetic arm for self-feeding. Nature *453*, 1098–1101.

Wessberg, J., Stambaugh, C.R., Kralik, J.D., Beck, P.D., Laubach, M., Chapin, J.K., Kim, J., Biggs, S.J., Srinivasan, M.A., and Nicolelis, M.A. (2000). Real-time prediction of hand trajectory by ensembles of cortical neurons in primates. Nature *408*, 361–365.

Zhang, H. (2004). The optimality of naive Bayes. Proc. Seventeenth Int. Florida Artif. Intell. Res. Soc. Conf. FLAIRS 2004 *1*, 1–6.